

pubs.acs.org/journal/abseba Article

# Automated Addressable Microfluidic Device for Minimally Disruptive Manipulation of Cells and Fluids within Living Cultures

Anh Tong, Quang Long Pham, Vatsal Shah, Akshay Naik, Paul Abatemarco, and Roman Voronov\*



Cite This: https://dx.doi.org/10.1021/acsbiomaterials.9b01969

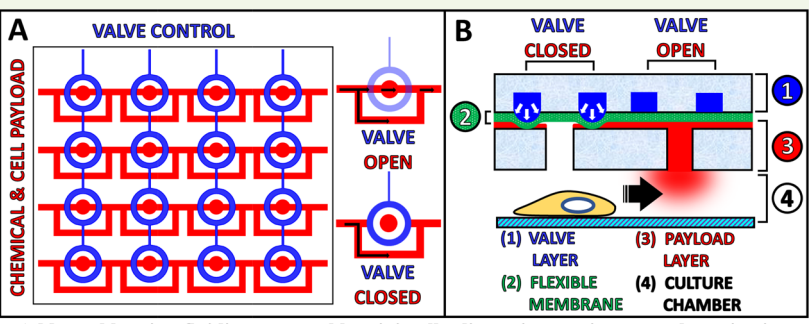


**ACCESS** 

III Metrics & More

Article Recommendations

s Supporting Information



Addressable microfluidic ports enable minimally disruptive spatiotemporal monitoring and controls via additive and subtractive cell and fluid manipulations in living cultures.

ABSTRACT: Cell culturing experiments are ubiquitous to the study of biology, development of new medical treatments, and the biomanufacturing industry. However, there are still major technological barriers limiting the advancement of knowledge and ballooning the experimental costs associated with these systems. For example, currently, it is difficult to perform nondisruptive monitoring and control of the cells in the cultured samples. This often necessitates the use of sacrificial assays and results in product inconsistency. To resolve these bottlenecks, we present a prototype "addressable" microfluidic technology capable of spatiotemporal fluid and cell manipulations within living cultures. As a proof-of-concept, we demonstrate its ability to perform additive manufacturing by seeding cells in spatial patterns (including co-culturing multiple cell types) and subtractive manufacturing by removing surface adherent cells via the focused flow of trypsin. Additionally, we show that the device can sample fluids and perform cell "biopsies" (which can be subsequently sent for ex situ analysis), from any location within its culture chamber. Finally, the onchip plumbing is completely automated using external electronics. This opens the possibility of performing long-term computerdriven experiments, where the cell behavior is modulated in response to the minimally disruptive observations (e.g., fluid sampling and cell biopsies) throughout the entire duration of the cultures. A limitation of the presented  $\alpha$  prototype is that it is only twodimensional (2D). However, technology serves as a foundation for ultimately extending the concept to three-dimensional (3D). Another limitation of the device is that it is currently made from poly(dimethylsiloxane) (PDMS), while more work needs to be done to manufacture from a material that degrades away or allow the cells to lay down the tissue matrix. Unfortunately, the existing biodegradable materials are typically not strong enough for the fabrication of microfluidic valves. Hence, new ones need to be developed before this technology can become mainstream. Yet, it is the hope of the authors that this will be achieved soon, and the microfluidic plumbing technology will eventually be scaled up to 3D, to overcome the limitations of the conventional cell culturing platforms.

**KEYWORDS:** automation, microfluidics, cell culturing, tissue engineering, biopsy, wound healing, patterning, control, additive manufacturing, subtractive manufacturing, fluid manipulation, cell manipulation, noninvasive, nondestructive, nondisruptive, scaffolds

#### I. INTRODUCTION

Cell cultures are estimated to become a \$6.5 billion market by 2022, with the biggest growths in drug discovery, biopharmaceutical production, toxicology, cosmetics, and stem cell research. <sup>1,2</sup> This financial incentive has helped to develop the culturing process from being messy, laborious and expensive, to much more organized through a broad range of commercial tools (e.g., bioreactors). However, the analysis and modulation

Received: December 25, 2019 Accepted: February 12, 2020 Published: February 12, 2020



of the cell behavior in these in vitro systems still face major technological bottlenecks, which limit the type of experiments that can be done using the cell cultures and balloon their costs:<sup>3</sup>

- (1) Sacrificial analysis—due to the inability to sample cells and fluids within living cultures nondestructively and because live long-term three-dimensional (3D) microscopy is challenging. This makes it necessary to perform destructive testing at the conclusion of each experiment, such as histological sectioning or crushing the sample for plate reader assays. As a result, a different culturing experiment must be performed for each new time point. This inflates the cost of the biological studies and slows down scientific progress tremendously.
- (2) Product variability—due to the absence of native supervision over the behavior of cells and lack of access to them post-seeding, there is no orchestration over the cell actions within the cultures. For example, even if one were to bioprint (i.e., deposit the cells into precise locations within a supporting material) the perfect artificial culture, the cells within it would be free to do a number of undesirable things afterward: (a) migrate away uncontrollably, (b) differentiate into the wrong lineage (e.g., spinal cord stem cell therapy turned into mucous tissue instead),5 and (c) deposit extracellular matrix (ECM) in the wrong locations and occlude the culture pores. All of these lead to nonviable cells and poor product consistency. In fact, a survey of 16 big pharmaceutical companies found that product consistency is possibly the single greatest challenge facing the cell culturing industry today.
- (3) Technology adoption barriers—even if one could generate the perfect cell culture in an academic laboratory, training industry (e.g., company, hospital, military) staff in custom culturing protocols for each new product remains another critical hurdle slowing down the biomanufacturing technologies from entering the commercial market. Therefore, a new approach to cell culturing is needed.

In this study, we hypothesize that to overcome these obstacles, an ideal culturing platform should be composed of the following elements: (1) active "vasculature" for distributing metabolites and clearing waste throughout living cultures; (2) nondestructive sampling of the cells and of the fluids from within the living cultures for an ex situ chemical analysis; (3) long-term live microscopy observation of the cell behavior and ECM synthesis; (4) culture modulation via cell and bioactive chemical (e.g., chemoattractants, growth and differentiation factors, drugs, etc.) delivery, to minimize product variability; and (5) automated spatiotemporal control over the culture development in a closed-loop manner, based on optical and chemical assaying feedback, to enable computer-driven culturing. The overall idea is depicted in Figure 1.

We further hypothesize that these goals can be achieved by merging microfluidics and cell culturing technologies. Interestingly, the microfluidic technologies share many characteristics with the conventional culture generation and development techniques, while at the same time lacking their major bottlenecks (see Table 1). Namely, they can seed cells with precision, perform nondestructive localized chemical sampling, and are transparent to microscopic observation. Moreover, the microfluidic substrates can be fabricated from a wider range of materials and with even higher precision than their bioprinted counterparts because there is no danger of damaging the cells

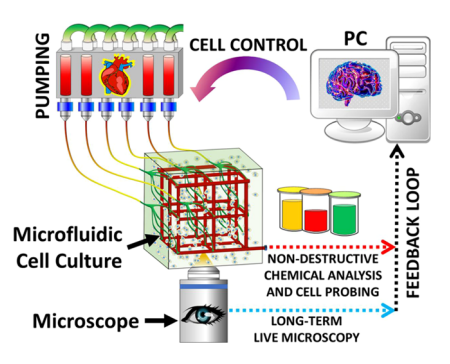


Figure 1. Envisioned microfluidic cell culturing platform with an active vasculature that enables targeted real-time minimally disruptive fluid and cell manipulations within the construct. External pumping acts like a "heart", which distributes metabolites and clears waste throughout the culture pore space. The entire experiment is orchestrated by a computer acting like a "brain". The computer's closed-loop responses are based on feedback from the nondestructive chemical analysis. Also, the feedback is ideally validated via long-term in situ automated live microscopy in small (i.e., optically transparent) sample sizes throughout the entire duration of the culture. As a result, the culturing experiment is closed-loop-controlled with a machine precision and reproducibility.

during the device fabrication process (since they can be flowed in afterward). Most importantly, the active vasculature of microchannels allows continuous nutrient delivery/waste removal and enables targeted modulation of cell behavior in a closed-loop manner.

In contrast, bioprinting is limited to the materials that are compatible with the living cells. The materials are typically soft (e.g., hydrogels) so that they can be extruded and later hardened via cross-linking. Furthermore, the extrusion can worsen the cell viability because the cells must survive the culture manufacturing process that may involve high shear forces, thermal stress, and/or toxic cross-linking agents. Moreover, the manufacturing resolution of the bioprinters is limited by the fact that the nozzle must be big enough to allow the cells to pass through it without getting damaged (i.e., typically >100  $\mu$ m diameter). Likewise, decellularized organs are limited to just the natural ECM material and structure. And for both, this and the artificial scaffold, methods, there is little control over where the cells are seeded. Finally, all three of the conventional approaches to generating cell cultures result in passive pores, which cannot be used for in situ cell analysis or control.

Therefore, the addition of the microfluidic plumbing provides numerous advantages over the conventional cell culturing approaches. Furthermore, although fabricating microfluidic devices (especially 3D ones) has been a major bottleneck to their adoption, 3D printers are on the verge of being able to manufacture them seamlessly. Hence, it makes sense to integrate cell culturing devices with microfluidic technologies, in anticipation of the near future when the advancements in 3D printing will facilitate their translation to the market.

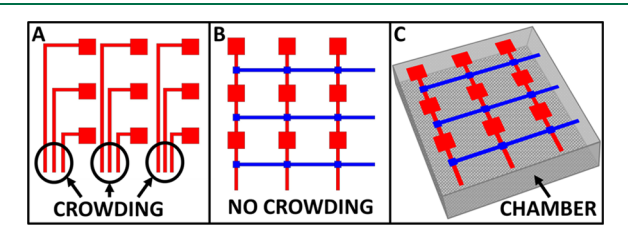
To that end, several such attempts have been made in the past. 9-17 However, these mostly focused on developing the materials and the fabrication techniques for the manufacturing of the microfluidic culturing devices, while the plumbing necessary for the targeted fluid and cell manipulation within them has not been designed. Specifically, the internal plumbing of such devices should contain dedicated ports, distributed at targeted locations (from here on termed as "addresses"), to enable the localized nondestructive manipulation (i.e., delivery/

Table 1. Comparison of Existing Biomanufacturing Technologies (Rows 1-3) with the Proposed Microfluidics Approach (Bottom Row)<sup>a</sup>

| tech type               | material         | geometry                            | fabrication         | seeding   | viability           | vasculature | analysis    | controls    |
|-------------------------|------------------|-------------------------------------|---------------------|-----------|---------------------|-------------|-------------|-------------|
| artificial scaffold     | any +            | poor to precise, micro to macro X/+ | easy to<br>hard X/+ | random X  | excellent +         | passive X   | bulk X      | bulk X      |
| decellularized<br>organ | natural O        | natural, micro to macro O           | medium O            | random X  | excellent +         | passive X   | bulk X      | bulk X      |
| bioprinting             | very-limited X   | precise, meso +                     | easy +              | precise + | poor to<br>good X/+ | passive X   | bulk X      | bulk X      |
| microfluidics           | less-limited X/O | precise, micro to meso +            | hard X              | precise + | excellent +         | active +    | localized + | localized + |
|                         |                  |                                     |                     |           |                     |             |             |             |

"+ = key advantages, X = fundamental limitations; O = neutral or no advantage. Micro =  $0.1-10 \mu m$ , meso =  $0-1000 \mu m$ , and macro =>1 mm.

probing) of cells and fluids within the cultures. Yet, this is a significant challenge because the plumbing should be both scalable to large culture sizes and at the same time be capable of maintaining a high-density targeting throughout its pore space. The problem is illustrated using a two-dimensional (2D) example in Figure 2A.



**Figure 2.** Difference in scalability and resolution of the addressable microfluidic arrays, illustrated using a  $3 \times 3$  grid example: (A) inefficient  $X \times Y$  scaling and the resolution limitations due to crowding of the supply channels; (B) efficient (X + Y) scaling, and the resolution is not limited by the crowding. (C) The plumbing from (B) connected to a single culturing chamber (gray). Red = flow channels through which cells or chemicals are delivered and/or sampled; blue = blocking (i.e., valve-actuating) channels.

In this figure, a naive approach is shown, where a  $3 \times 3$  grid of microfluidic ports is actuated via a separate channel dedicated to each of the addresses. This suffers from: (a) poor scaling—the number of flow channels required to actuate each individual address in the grid scales as  $X \times Y$ , which is the worst-case scenario and (b) crowding—the spacing available for the channels is limited by the separation distance between the neighboring columns of addresses (which should be as small as possible, to ideally be able to manipulate and analyze the culture with a single-cell spatial resolution). Fortunately, an old concept in the field of microfluidics solves this problem by including orthogonally blocking channels, <sup>18–20</sup> shown in blue in Figure 2B. By using this combination of flow and blocking (i.e., valve actuating) channels, (X + Y) scaling is achieved (i.e., only three flow + three blocking channels are required, as opposed to a total of nine dedicated flow channels in the  $X \times Y$  scaling), and the resolution is no longer limited by the crowding.

Thus, the "addressable" microfluidic technologies, such as in Figure 2B, yield the best possible scaling (e.g., microfluidic chips with over 1000 addresses have been made<sup>21–24</sup>), and the address density is no longer limited by the crowding. Therefore, this type of plumbing is the best choice for large-sized cultures. Yet, it has not been used in the microfluidic culturing devices before. <sup>9–17</sup> Instead, the addresses typically serve as separate isolated chambers on chips used for multiple parallel experiments, for example, an array of cell culturing chambers for high-throughput drug testing, <sup>18</sup> a droplet-based device for multiparameter

analysis of single microbes and microbial communities, <sup>19</sup> and a stencil for protein and cell patterning of substrates. <sup>20</sup>

However, here we are interested in achieving addressable cell and fluid manipulations within a single culturing chamber (see Figure 2C), which has not been done before. Furthermore, we want the device to be automated to enable computers to perform the manipulations over long-time culturing experiments. To that end, the remainder of the manuscript presents our proof-of-concept platform, which adapts the addressable microfluidic plumbing and automation, in order to perform the minimally disruptive cell and chemical manipulations needed to revolutionize the advanced cell culturing technologies.

#### II. METHODS AND EXPERIMENT

II.I. Master Mold Fabrication. The device was fabricated via a multilayer soft-lithography technique  $^{25}$  using a custom-built UV mask aligner.26 The device's design is discussed in detail in Section III.I(see Figures 6 and 7). The molds for the device was fabricated using a negative photoresist (SU-8, MicroChem, Westborough, MA, Cat.# Y111077 1000L1GL, Cat.# Y111072 0500L1GL, and Cat.# Y111070 0500L1GL) and a positive photoresist (AZ P4620, Integrated Micro Materials, Argyle, TX, Cat.# 10567123157). First, the microscale pattern was sketched using AutoCAD (Autodesk, Mill Valey, CA) and printed at 50 800 dpi on transparency (Fineline Imaging, Colorado Springs, CO) to generate a high-resolution photomask. Initially, the 4 in. silicon wafers (University Wafer, Boston, MA, Cat.# 452) were washed carefully with diluted soap, rinsed with acetone, methanol, and deionized (DI)-water (AMD solvents), dehydrated at 180 °C for 15 min. Subsequently, the wafers were cooled down to room temperature and treated with hexamethyldisilazane (HMDS) (Alfa Aesar, Tewksbury, MA, Cat.# 999-97-3) to enhance the photoresist adhesion. The procedures to create the master mold for each layer of the microfluidic device are described below:

II.I.I. Payload Layer. The master mold for the flow layer consists of two types of photoresists, positive photoresist AZ P4620 for the flow channels and negative photoresist SU-8 2150 (MicroChem, Westborough, MA, Cat.# Y111077 1000L1GL) for the addressable ports. Round profile flow channels (see Figure 3A)—AZ P4620 was spincoated at 1400 rpm and soft-baked at 90 °C for 10 min. Then, the second layer of AZ P4620 was spin-coated on the same wafer to reach the target coated layer of 28  $\mu m$  and soft-baked at 90 °C for 1 h. Subsequently, the wafer was rehydrated overnight inside the oven at 37 °C with an opened water tray (12 h), exposed to UV light (exposure dose: 2800 mJ cm<sup>-2</sup>) and developed by immersing them in a vessel containing AZ 400 K developer for 10 to 15 min (Integrated Micro Materials, Argyle, TX, Cat.# 10063823163) to form 28 μm height features. The round profile of the channels was created by baking the wafer with AZ P4620 features at 150 °C on a programmable hotplate for 15 h, starting at 65 °C with a heating ramp rate of 4 °C h<sup>-1</sup>. Addressable ports (see Figure 3B)-SU-8 2150 was spin-coated directly on the same wafer at 1250 rpm, aligned with the first pattern using a custom mask aligner, 26 exposed to the UV (exposure dose: 600 mJ cm<sup>-2</sup>), and developed by immersing them in a vessel containing SU-8 developer (MicroChem, Westborough, MA, Cat.# Y020100) for 30 min to generate 550  $\mu$ m height square features for the addressable ports. The

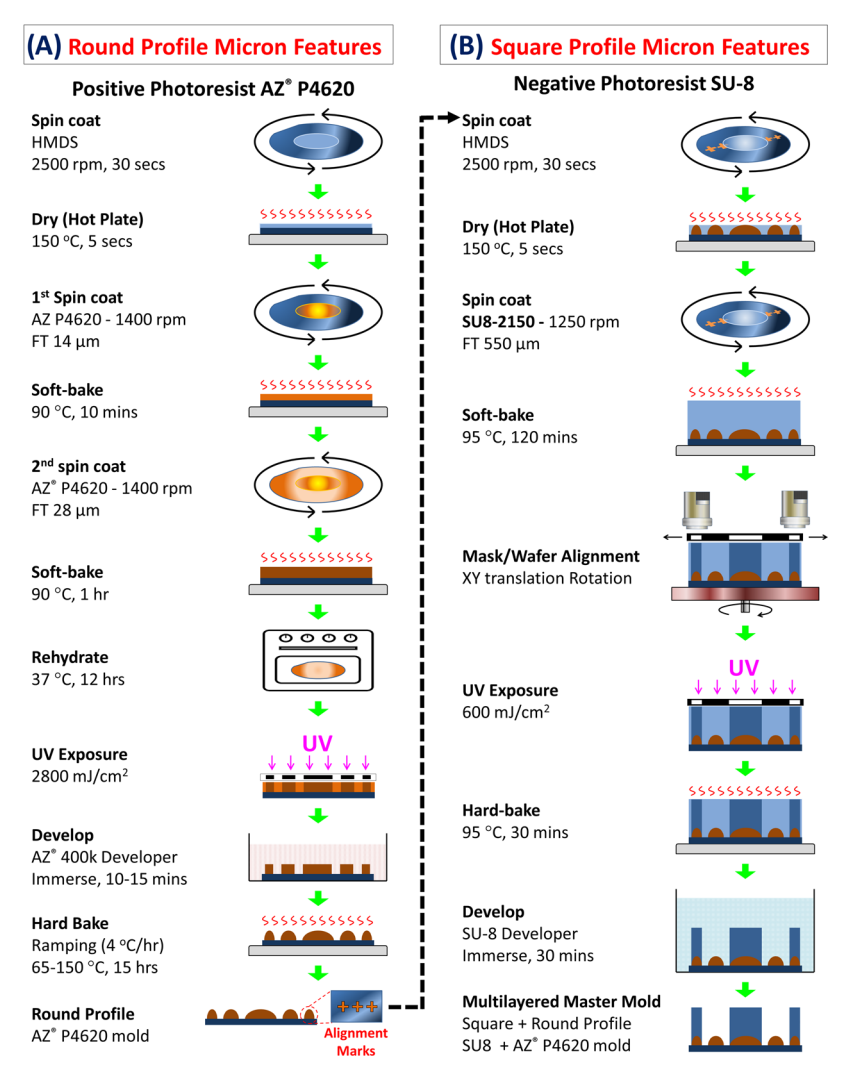


**Figure 3.** Schematic showing the step-by-step fabrication process of a multilayered master mold, composed of two different heights/profiles (round and square) of micron-sized features on a 4 in. silicon wafer. The fabrication essentially follows standard photolithography procedures, such as spin coating, UV exposure, and developing. (A) Positive photoresist AZ P4620 template is first created, and the developed photoresist is then reflowed by baking at 150 °C, to achieve the round profile features. Alignment marks are also imprinted on the two sides of the wafer to be used in the next step. (B) SU-8 photoresist layer is patterned on the same wafer. Prior to the UV exposure, the alignment marks on the template photomask and on the silicon wafer are aligned using the custom mask aligner.<sup>26</sup> Abbreviations: FT = film thickness.

developed photoresist was fully cross-linked at 180 °C for 2 h, cooled down to room temperature, and treated with perfluorodecyltrichlorosilane (FDTS) (Alfa Aesar, Tewksbury, MA, Cat.# 78560-44-8) inside a vacuum desiccator chamber for 4 h.

*II.I.I.* Control Layer. There were two control layers in the addressable device. The first one was used to actuate the valves in the payload layer (Figures 4 and 6A), and the second one was to open/close inlets and outlets of the culture chamber (Figures 4 and 7). The photomasks were switched for each layer, and the procedure to create the master mold for the control layer remained the same. Specifically, SU-8 2050 (MicroChem, Westborough, MA, Cat.# Y111072 0500L1GL) was spin-coated at 1500 rpm, exposed to UV light (exposure dose: 240 mJ cm<sup>-2</sup>), and developed on a 4 in. silicon wafer to generate a 120  $\mu$ m height pattern. The developed photoresist was fully cross-linked at 180 °C for 2 h and then slowly cooled down to room temperature.

II.I.II. Culture Chamber. The master mold for the culture chamber also consisted of two types of photoresists, positive photoresist AZ P4620 for features, which overlapped with the control valve layer, and negative photoresist SU-8 2150 for the cell culture chamber and nonoverlapping flow channels. The round profile features were created by following the same procedure as the round profile flow channels for the payload layer (see above). Then, SU-8 2035 (MicroChem, Westborough, MA, Cat.# Y111070 0500L1GL) was spin-coated at

1500 rpm, exposed to UV light (exposure dose: 210 mJ cm $^{-2}$ ), and developed on a 4 in. silicon wafer to generate an 85  $\mu$ m height square pattern. The developed photoresist was fully cross-linked at 180 °C for 2 h and then slowly cooled down to room temperature.

II.II. Microfluidic Device Fabrication. Different poly-(dimethylsiloxane) (PDMS) Sylgard 184 (Dow Corning Corporation, Midland, MI, Cat.# 2065622) layers of the device were generated using soft lithography. The elastomer with a base-to-agent ratio of 10:1 was poured over the photopatterned mold to reach the thickness of 5, 1, and 2 mm for the payload's control layer, the culture chamber's control layer, and the culture chamber, respectively. Then, the PDMS-casted molds were degassed inside the vacuum desiccator chamber for 2 h and followed by curing on a hotplate at 65 °C overnight (12 h). The PDMS flexible membranes (Figures 4 and 6B) of 35  $\mu$ m thickness were created by spin coating the PDMS with a 20:1 base-to-agent ratio onto 4 in. silicon wafer at 2500 rpm for 60 s and then baked at 65 °C for at least 1 h. The cells and/or chemical payload layer were created by following an established PDMS stencil procedure.<sup>20</sup> Then, all of the layers were peeled off from the master molds, washed with diluted soap, rinsed with AMD solvents, dried on a 180 °C hotplate, treated with air plasma, and bound to each other using our custom-built PDMS desktop aligner<sup>27</sup> to form the multilayered microfluidic device (Figure 4). During the PDMS bonding process, a biopsy punch (Electron Microscopy Sciences, PA,

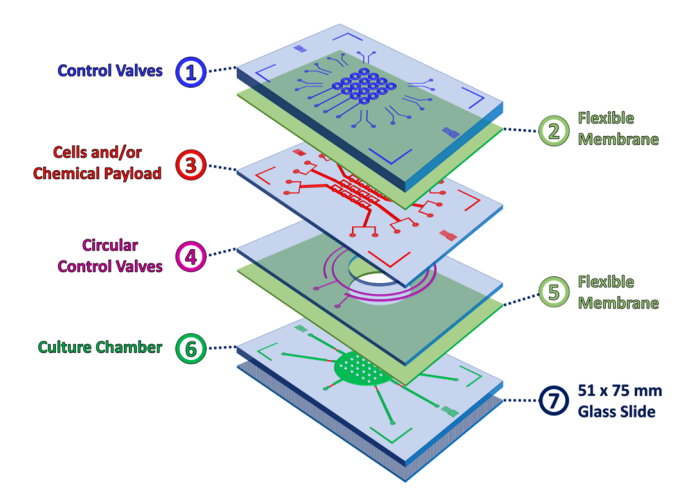


Figure 4. Diagram showing how the addressable microfluidic device is created by stacking seven different layers on top of each other. (1) Cells and/or chemical payload's control valve layer; (2) 35  $\mu$ m flexible membrane; (3) cells and/or chemical payload with addressable port layer; (4) control layer for the culture chamber with a 12 mm in diameter punch-through hole at the center; (5) 35  $\mu$ m flexible membrane with a 12 mm in diameter punch-through hole at the center; (6) culture chamber; and (7) 51 × 75 mm² glass slide.

Cat.# 69039-05) with a diameter of 0.5 mm was then used to create punch-through inlet and outlet ports for tubing connections. The order of binding single layers to form the multilayered microfluidic device was as follows: (1) cells and/or chemical payload's control valve layer; (2) 35  $\mu$ m flexible membrane; (3) cells and/or chemical payload channels with an addressable port layer; (4) control valve layer for the culture chamber; (5) 35  $\mu$ m flexible membrane, (6) culture chamber; (7) substrate consisting of a 51 × 75 mm² glass slide (Corning, Corning, NY, Cat.# 2947-75X50) to which the device was bound to using air plasma. Note that a puncher (12 mm in diameter) was used to create through a hole at the center of layers 4 and 5, to generate an interconnection between the payload layer and the culture chamber.

II.III. Pumping Automation, Experimental Setup, and Microscopy. Here, we employed a modification of an open-source programmable pneumatic pumping technology, developed for operation and automated control of single- and multilayer microfluidic devices. <sup>28–30</sup> Following this design, we built a custom pneumatic pumping system based on modular industrial automation components made by WAGO (see Figure 5A). Specifically, the core of the setup consisted of an Ethernet-based programmable WAGO-I/O-SYSTEM 750 logic controller and an eight-channel digital output module (WAGO Kontakttechnik GmbH & Co., Minden, Germany, Cat.# 750-530) that allows the controller to drive 24 V Festo (MH1-A-24VDC-N-HC-8V-PR-K01-QM-APBP-CX-DX, Festo, Germany, Cat.# 197334) miniature pneumatic solenoid valves (see Figure 5B). The solenoid

valves were connected to a custom DYI pneumatic pumping system (see Figure 5C), which is used to manipulate cells and fluids at the addresses. To avoid contact between the solenoid valves and the pumped liquid, the system contains machined reservoirs (see Figure 5D) that prevent water from backing up into the former. The solenoid valves are actuated by sending 24 V signals to them via an eight-channel digital output module (Wago 750-530). The "on" and "off" positions of the solenoid valves correspond to the "open" and "close" states of the valves on the chip. Switching from open to close means changing the pressure inside the on-chip valve from atmospheric pressure to 20 psi, respectively. The device was connected to PYREX 100 mL round media storage bottles (Corning, Corning, NY, Cat.# 1395-250) with solvent bottle cap, GL45, 5 Luer ports (Cole-Parmer, Vernon Hills, IL, Cat.# EW-12018-11) and house-air via Tygon tubing (Cole-Parmer, IL, Cat.# SI-06419-01) of 0.02 in. inner diameter. The valves in the control layers were also automatically actuated via the miniature pneumatic solenoid valves that were operated by the programmable WAGO controller. The controller was connected to a computer via an Ethernet interface. First, a sequence of patterns to be addressed on the device was specified by a user using a custom Matlab graphical user interface (GUI) (see Figure 5E). Then, these patterns were sent to the WAGO module to toggle the Festo valves, which in turn selectively actuated the on-chip valves at the preset locations (specified by the pattern created above) for the delivery of the payloads and collection of samples through the ports.

The device was mounted on an automated microscope (Olympus, Japan, model IX83) equipped with an XY motorized stage (Ludl, Hawthorne, NY, Cat.# 96S106-O3-LE2) and a custom temperature control setup. Images were acquired using a digital complementary metal oxide semiconductor (CMOS) camera (Orca Flash 4.0 V2, Hamamatsu, Japan, Cat.# C11440-22CU). The image acquisition was performed using a custom Matlab (MathWorks Inc., Natick, MA) GUI.<sup>31</sup> The image processing was parallelized using Matlab's Distributed Computing Toolbox to enable an on-line analysis of the culture

II.IV. Demonstration of Fluid Manipulation within the **Device.** Since many biochemical agonists are colorless/undetectable by regular microscopes, food dye (Assorted Neon!, McCormick, Baltimore, MD) was used to create a visual demonstration of the fluid manipulations within the microfluidic device. The dye was added into the media bottles connected to the flow channels of the device via Tygon tubing. Air pressure of ∼1 psi was used to drive the fluid into the device and across the flow channels. On-chip valves were connected to a pressure source of  $\sim$ 20 psi to fully obstruct the flow when the valves were in a "closed" state. Matlab code was used to preset the pattern in which the dye was delivered and sampled. For the latter, the one outlet of the payload channel was connected to vials under negative pressure via Tygon tubing, in which the chemicals (food dyes) were withdrawn back via a port at any (either at the same or at a different) location of the 4 × 4 array via pressure reversal into the sample collecting vials for further analysis. The time-lapse video of the dye delivery was recorded using a compact digital microscope (Dino-Lite, Torrance, CA, Cat.# AD4113T).

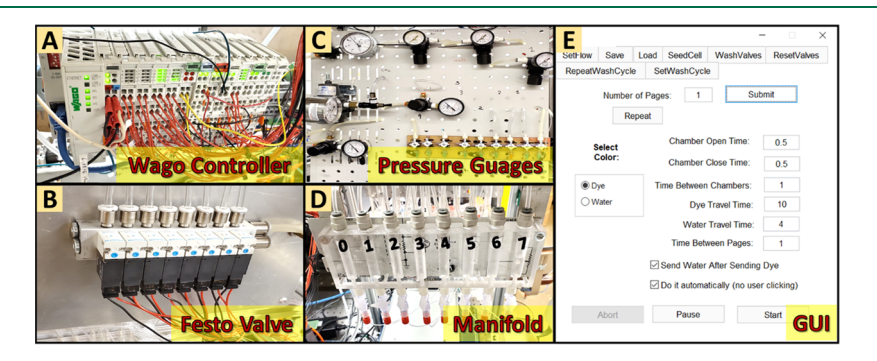


Figure 5. Automated pumping system. (A) Wago controller; (B) manifold with eight Festo solenoid valves; (C) pneumatic pumping system; (D) water storage machined reservoirs for control channels; (E) custom GUI for controlling the solenoid valves via the Wago controller.

**II.V. Demonstration of Cell Manipulation within the Device.** *II.V.I. Device Preparation for Cell Culturing.* The device was autoclaved at 121 °C for 60 min to completely cure the non-cross-linked oligomers inside the bulk PDMS, evaporate the remained solvent from the curing agent, and sterilize the PDMS device prior to the adhesive surface treatment and cell seeding. Subsequently, the cell culture chamber of the device was coated with fibronectin ( $10 \,\mu g \, \text{mL}^{-1}$ ) (Corning, Corning, NY, Cat.# 47743-654), and the internal surfaces of the microfluidic channels were treated with 2% bovine serum albumin (BSA) (Sigma, St. Louis, MO, Cat.# A2153) at 25 °C for at least 10 h inside the UV chamber to maintain the sterile condition of the PDMS device. In this case, 2% BSA solution was used to prevent the adhesion of the cells to the microfluidic channel's surface.  $^{32,33}$ 

II.V.II. Cell Preparation. Culture media was prepared from the minimum essential medium (MEM) (Sigma, St. Louis, MO, Cat.# M0894-10X1L) supplemented with 10% (v/v) fetal bovine serum (FBS) (Bio-Techne, Minneapolis, MN, Cat.# S11550) and 1% (v/v) penicillin-streptomycin (10 000 U mL-1) (Thermo Fisher, Waltham, MA, Cat.# 15140122). Basal media was composed of MEM supplemented with 1% (v/v) penicillin-streptomycin. For incubation in a 5% CO<sub>2</sub> atmosphere, the medium was buffered by 26 mM sodium bicarbonate (Sigma, St. Louis, MO, Cat.# S5761). CO<sub>2</sub>-independent media buffered by 20 mM N-(2-hydroxyethyl)piperazine-N'-ethanesulfonic acid (HEPES) (Sigma, St. Louis, MO, Cat.# H0887) were used for microscope stage-top experiments. Mouse bone marrow-derived mesenchymal stem cells (MSCs) (S1502-100, strain: C57BL/6) and mouse embryo fibroblasts (NIH/3T3) (ATCC CRL-1658TM, strain: NIH/Swiss) were used for this study. The selected cell types were suspended in a prewarmed complete growth minimum essential medium (MEM), supplemented with FBS and 1% (v/v) penicillinstreptomycin, to reach the cell concentration of  $5 \times 10^6$  cells mL<sup>-1</sup>. Initially, the cells were trypsinized from a T-75 cell culture flask by adding 2 mL of 1× trypsin/ethylenediaminetetraacetic acid (EDTA) (0.25%, 0.2 g L<sup>-1</sup> EDTA) (Corning Inc., Corning, NY, Cat.# 45000-660) for 3 min. MEM culture media with 10% FBS (8 mL) was added to neutralize the trypsin/EDTA activity. The cell suspension was centrifuged at 1000g for 2 min. The supernatant was removed by aspiration, and the cell pellet was resuspended in 5 mL of CellTracker fluorescent dye CellTracker CM-DiI (Invitrogen, Waltham, MA, Cat.# C7000) in phosphate-buffered saline (PBS) (1× without calcium and magnesium) (Sigma, St. Louis, MO, Cat.# D8537) for: (1) red fluorescence cell membrane labeling ( $\lambda_{\rm exc} = 553 \text{ nm}/\lambda_{\rm em} = 570 \text{ nm}$ ), CellTracker Green CMFDA dye (Invitrogen, Waltham, MA, Cat.# C2925), or (2) green fluorescent cell cytoplasm labeling ( $\lambda_{\rm exc}$  = 492  $nm/\lambda_{em} = 517$  nm). The cell suspension was incubated at 37 °C for 45 min and then centrifuged at 1000g for 2 min. The supernatant was removed by aspiration, and the cell pellet was resuspended in MEM culture media to reach the desired concentration (5  $\times$  10<sup>6</sup> cells mL<sup>-1</sup>). Finally, the cell suspension was ready for the cell seeding procedure.

II.V.III. Additive Manufacturing. Suspended cells (10 mL) were added to a dispensing bottle with four ports that were connected to the cell and/or chemical payload layer channels of the device. The bottle was then pressurized via 5% carbon dioxide at 6-7 psi, under a constant shaking motion at 210 rpm. The on-chip valves were connected to a pressure source of ~20 psi to fully block the flow to an address when the valves are in a closed state. The Matlab GUI was used to predetermine the patterns, in which the cells were seeded via the addressable ports. The fluorescent and time-lapse images were captured using a fully automated Olympus IX83 microscope fitted with a 20× phase-contrast objective (Olympus, Japan, Cat.# UPLFLN20XPH) and a CMOS camera (Orca Flash 4.0 v2, Hamamatsu, Japan, Cat.# C11440-22CU). Time-lapse images were automatically captured at a 15 min interval for a duration of 30 h. For each time step, 121 tile images (size: 662.07 × 662.07  $\mu$ m<sup>2</sup>) were acquired at different locations, stitched, and stabilized using an in-house Matlab 2016b code (MathWorks, Inc., Natick, MA). During the acquisition, the culture media was automatically refreshed every 5 h via the culture chamber's flow channels of the device by actuating the control valves in that layer on and off. The composite images of the patterned cell co-cultures created

by seeding two different cell types in different locations were assembled using the ImageJ software (National Institutes of Health).<sup>34</sup>

<code>II.V.IV.</code> Subtractive Manufacturing. The suspended cell solution at a concentration of  $(0.6 \times 10^6 \text{ cells mL}^{-1})$  was delivered into the culture chamber until the cells were uniformly seeded. After cultivation at 37 °C for 3 h, PBS (1× without calcium and magnesium) was used for flushing the cell culture chamber for 30 s and trypsin (0.25% trypsin 0.2 g L $^{-1}$  EDTA) was then delivered into the culture chamber through user-specified addresses for 10 min. The bond cleavage effectiveness was gauged based on real-time observation of cell morphology via microscopy. After the digestion, the lifted cells were flushed away by continually flowing the PBS through the same address. Pulsatile flow with a periodicity of every 0.5 s was used to facilitate the cell detachment from the substrate floor of the culture chamber.

II.V.V. Minimally Disruptive Cell Biopsies. The cells were uniformly seeded in the culture chamber and treated with trypsin for 5 min (following the procedure in the previous Section II.V.IV) until they were partially detached. Eventually, the detached cells were collected from the culture chamber through the microfluidic ports via pressure reversal applied at the outlet of the payload channel. Subsequently, the collected cells were stored outside of the device so that they could be used for the ex situ analysis without affecting the main culture.

#### III. RESULTS

III.I. Redesigned Microfluidic Plumbing for Addressable Access to the Culture Chamber. In this manuscript, we have realized an envisioned proof-of-concept automated microfluidic platform, capable of minimally disruptive *XY* fluid and cell manipulations within living 2D cultures. To do this, we used a combination of microsized flow channels and blocking pneumatic valves, to actuate the individual addresses independently of each other. After going through multiple iterations of modifying the published addressable plumbing designs, <sup>18–20</sup> we have converged upon the result shown in Figure 6A. There, the

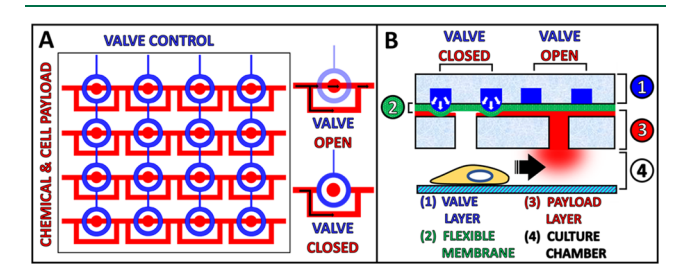


**Figure 6.** Schematic of the addressable microfluidic plumbing developed in this manuscript. (A) Top XY view of a 4  $\times$  4 matrix of the addressable ports. Flow channels are shown in red and blocking valve channels are in blue. The inset shows that a port is active when the valve is open and bypassed when it is closed. Black arrows indicate the direction of flow, which assumes a payload delivery to (as opposed to sampling at) an address. (B) Z cross section of the same device, showing how a cell neighboring an active microfluidic port is attracted to it due to the chemoattractant released into the culture chamber at that location. At the same time, it is shown that the inactive port directly above the cell does not affect its behavior, since no chemical payload is being delivered through this address.

addressable array has a  $4 \times 4$  size for simplicity, though the actual grid size is a free parameter. Each of the addresses in the array is shown as red discs, which are surrounded by O-shaped pneumatic valves (shown as blue circles). When the valve is closed (see the inset in Figure 6A), the fluid traveling through the red channels is rerouted around the address via a thin bypass channel (also labeled in red). However, when a valve is opened, the corresponding address can either deliver or withdraw (depending on the direction of the flow in the red channels) the

fluid carrying a chemical payload, and/or cells, to/from the culture chamber below (which is shown at #4 in Figure 6B).

Figure 6B shows a Z cross section of the device, which shows that it consists of four main layers (from top to bottom): a valve layer, a thin flexible membrane, a flow layer, and a cell culture chamber. The action of the O-shaped valve is also shown in the same figure: in the closed state, the pressurized valve expands, causing the flexible membrane to block flow to the address; conversely, in the open state, the flow is allowed to enter the address freely, where a microfluidic port then connects it with the culture chamber below. As an example, a chemical payload can be delivered through this port to attract a neighboring cell. At the same time, the closed port directly above the cell would not affect its behavior since no chemical is being released at that location. Furthermore, the same ports can be used to sample the culture media and seed or collect cells at different locations throughout the culture chamber.

Additionally, the culture chamber is supplemented with side channels for replenishing the media, uniform seeding of the cells, and flushing of the chamber. Figure 7 shows a zoomed out top

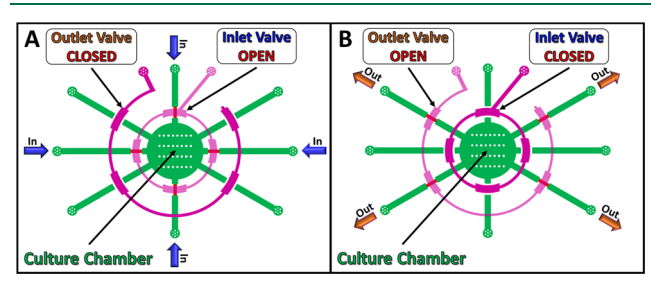


**Figure 7.** Top *XY* view schematic of the "culture chamber" with the "circular control valves." The culture chamber is shown in green, and the circular control valves surrounding it are in pink. (A) Fluid and cells can be added to the culture chamber through the four inlet channels (marked with blue arrows) when the inlet control valve is open and the outlet control valve is closed. (B) Conversely, the four outlet channels (marked with orange arrows) can be used to remove fluids and cells from the culture chamber when the inlet control valve is closed and the outlet control valve is open.

view of the culture chamber (labeled in green) and two surrounding circular valves (labeled in pink) that are introduced to control the flow in and out of the chamber via the side channels (also labeled in green). The mechanism of the circular valves is the same as the "O-shaped" control valves for the payload channels, except there are no bypass channels in this layer. Instead, the circular valves were designed to fully block the flow in or out of the culture chamber if necessary.

Like the automated operation of the addressable ports, the circular control valves can be opened or closed on demand using the control software (see Section II.III). This allows the device to replenish the old media in the culture chamber without the need to actuate the addressable ports. Specifically, fresh media can be delivered to the culture chamber through the inlets (see green arrows in Figure 7A) at fixed intervals (e.g., every 5 h) and old media can be flushed out through the outlets (see purple arrows in Figure 7B). Additionally, both control valves can be closed at the same time to prevent any fluid currents inside of the culture chamber. This is extremely important at the seeding stage, when the cells require a static condition to form focal adhesions with the substrate.

III.II. Nondisruptive Fluid Manipulation within the Culture Chamber. Some possible fluid and/or cell manipu-

lations within the device are: (1) seeding different cell types in varied amounts by flowing them into predetermined spatial patterns; (2) nourishing the cells in the culture chamber by continuously renewing the media; (3) inducing and directing cell migration by establishing a dynamic nutrient and/or a chemoattractant gradient; (4) patterning tissues by modulating cell differentiation and/or morphology via delivery of bioagonists (e.g., growth, differentiation factors) and/or drugs (e.g., cytoskeleton-altering) to specified locations/selected cells within the device; and (5) sampling a living culture non-disruptively by collecting and, sending off for analysis, effluents from different locations above the cells in the culture chamber.

The action of delivering and sampling chemicals within the addressable device is shown in the left and right panes of Figure 8, respectively. In the former case, a purple dye is delivered to the

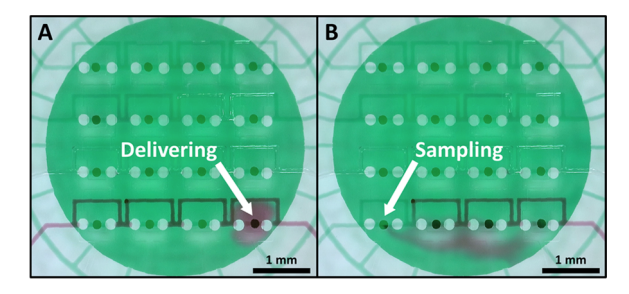


**Figure 8.** Microscopy of the fluid manipulation within the culture chamber. (A) Delivery of a purple dye to the bottom right corner port in the  $4 \times 4$  grid; (B) sampling of the delivered purple dye via the bottom left corner port in the  $4 \times 4$  grid. The culture chamber is filled with a green dye for contrast. Each port is 150  $\mu$ m in diameter, and the channels are 100  $\mu$ m in width. The view is from the top of the device.

right bottom corner of a  $4 \times 4$  array of microfluidic ports, while in the latter case, the same purple dye is withdrawn back via a port at the opposite end of the same address row. As a possible application, the picked-up fluid could be a cell culture effluent, which would then be sent off to an external sensor for *ex situ* analysis. This would eliminate the reliance on destructive chemical assays (e.g., histological sectioning or crushing the sample for plate reader analysis) and ensure continuous monitoring of the biology occurring within live cultures. Furthermore, this can be done continuously over long periods of time, given that the whole process is automated (and as such, does not require any human involvement). Video S1 shows the operation of the device over time, where the purple dye is delivered and sampled to/at different addresses within the  $4 \times 4$  grid of microfluidic ports.

III.III. Minimally Disruptive Cell Manipulations within the Culture Chamber. To further demonstrate the addressable device's ability to manipulate cells within the culture chamber, its ports were used for seeding (i.e., additive manufacturing) a co-culture of mouse MSCs and NIH/3T3s in a predetermined spatial pattern. Video S2 shows the process of the cell delivery through a single port to the culture chamber below, and Figure 9A shows the MSCs (green) seeded in a square shape that surrounds the NIH/3T3s (red) deposited in its center. In this figure, each of the addressable ports in the 4 × 4 grid from Figure 6A was used to deliver the different cell types to the culture chamber below.

Although the resulting resolution is slightly lower than that of a typical bioprinter (e.g.,  $100-300~\mu m$ ), it can be improved further by either reducing the feature size of the device's design

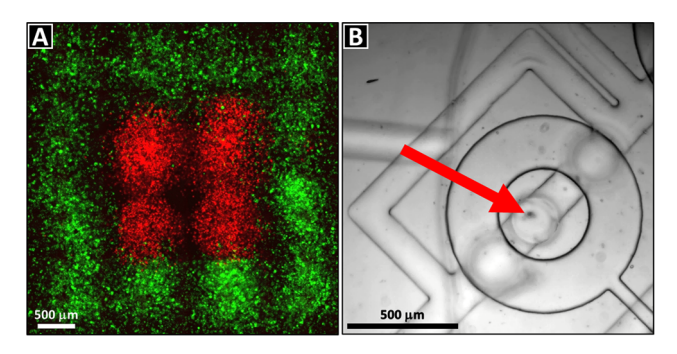


**Figure 9.** Minimally disruptive additive cell manipulations within the culture chamber of the device. (A) Fluorescence panorama showing MSCs (green) seeded in a square pattern, with NIH/3T3s (red) in its center. The panel size is  $\sim$ 4.5  $\times$  4.5 mm<sup>2</sup>. (B) Bright-field microscopy image showing the ability to trap and manipulate a single cell (red arrow) at a time.

or by controlling how many cells are being manipulated at a time. For example, Figure 9B and Video S3 show the device's ability to trap single cells by the O-valves surrounding its microfluidic ports. This means that, in principle, the additive manufacturing can be done with a single-cell precision (especially if machine vision-based automation is utilized). Alternatively, the seeding density can be controlled by varying the concentration of the cells in the carrier fluid and by changing how much of it can pass through an address while it is open. For example, Figure 10 shows a cell density gradient created by

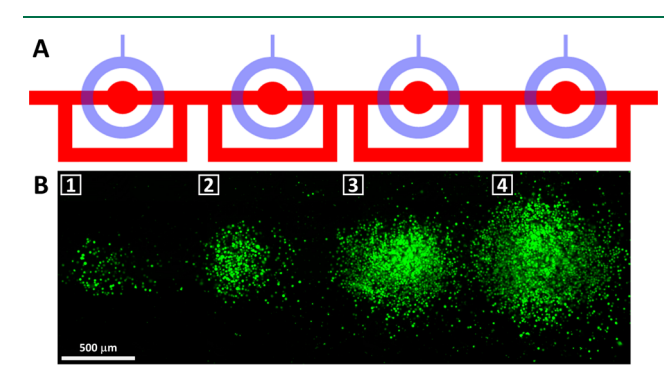


**Figure 10.** Cell seeding density gradient created by the device to demonstrate its utility in additive manufacturing. (A) Reference diagram showing the four addresses that were used for creating the cell seeding density gradient pattern. (B) Fluorescence microscopy of the MSC seeding gradient created in the culture chamber of the device, increasing in cell density from left to right. Panorama is  $\sim 1.3 \times 4$  mm<sup>2</sup>.

delivering MSCs to a row of addresses in progressively increasing amounts, from left to right. This was achieved by keeping the control valves open for progressively longer times during the cell delivery via flow: starting with 0.5 s for the leftmost address and then increasing the interval by 0.5 s for each subsequent location (ending with 2 s for the right-most one). Furthermore, the vertical distance between the addressable port and the substrate (i.e., the culture chamber's floor) and the height and the diameter of the ports (analogous to a bioprinter nozzle) can be modified to improve the resolution of cell patterning. For example, it has been shown that these parameters can be efficiently optimized to achieve high resolution and accuracy in cell additive manufacturing. <sup>35</sup>

Additionally, Figure 11 demonstrates the device's ability to create inverse cell patterns via subtractive manufacturing. The

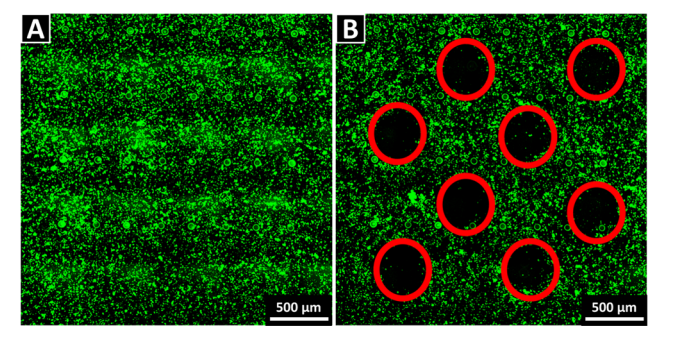


**Figure 11.** Fluorescence microscopy of minimally disruptive subtractive manufacturing: (A) culture chamber's "floor" covered with a confluent MSC layer (labeled using a fluorescent CellTracker Green CMFDA dye) below a 4 × 4 matrix of addressable ports, before the cell subtraction; (B) array of spaces (highlighted using red circles) from which the cells were removed via the subtraction (i.e., trypsinization followed by pulsatile flow). See Video S4 for an animation of the process at a representative addressable port.

idea is to first seed cells uniformly in the culture chamber and then let them adhere sufficiently to its floor to reach confluence (see Figure 11A). Subsequently, the focal adhesions anchoring the confluent cells to the bottom are cleaved by delivering a mixture of 0.25% trypsin 0.2 g  $\rm L^{-1}$  EDTA for a duration of 10 min. Eventually, the detached cells are flushed away via the flow of PBS from user-specified addresses to create localized clearings arranged in a spatial pattern in the culture below them (see Figure 11B). It should be noted that the PBS flow is at times pulsed to increase the detachment of the cells from the substrate (see Video S4).

This example of subtractive manufacturing demonstrates the ability of the device to remove undesired cell overgrowth and correct any localized seeding mistakes (something that is not possible with conventional scaffold and bioprinting approaches). Another possible application of this technology is the creation of contactless high-throughput wound healing assays. Specifically, in a typical assay, it is desirable to be able to create an artificial "wound" opening in a monolayer of a patient's cells grown to confluence. Subsequently, the cells surrounding the wound proliferate and migrate, eventually covering up the empty space and sealing the "injury". Typically, these wounds are created using mechanical (e.g., scratch, stamp), thermal, electrical, or optical damage to the cells.<sup>36</sup> Most recently, flow focusing using microfluidics has provided a contact-free alternative for selectively removing the cells enzymatically, to generate a wound with a clear boundary and without damaging the surrounding cells or the substrate's surface coating (which is often necessary for increasing cell adhesion and/or directing the culture's fate). 37-43 However, all of these assays yield only linear-shaped wounds, whereas the addressable technology reported in this manuscript can create circular ones (as in Figure 11B).

Finally, Video S5 shows the device's ability to perform minimally disruptive cell biopsies at different locations in the culturing chamber. This is inspired by how adherent single cells are trypsinized and then retrieved from cultures via micropipette suction. Similarly, in our device, the adherent cells are trypsinized using the same procedure as in the subtractive manufacturing. However, in this case, they are drawn into the addressable port above via a pressure reversal and are flowed away to a location outside of the culture chamber via the microfluidic channels. Subsequently, *ex situ* sacrificial analysis

can be performed on the collected cells without affecting the main culture in the device (e.g., see Figure S1).

Put together, these fluid and cell manipulation abilities demonstrate the versatility and the potential of our device to perform automated minimally disruptive observations within living cultures.

# IV. DISCUSSION

The goal of this work was to create a technology capable of realtime minimally disruptive manipulation of cells and fluids within living cultures. A major disadvantage of the existing biomanufacturing methods is the disconnect between the cell-substrate construct fabrication and its culturing: namely, once the cells are either seeded or bioprinted into the intended locations, all access to them is lost for the remainder of the culturing duration. As a result, the existing controls over the cell behavior are typically done in one of the following ways: (A) substrate—shape, stiffness, charge, porosity, and chemical composition are used to affect the cell fate and culture development; (B) biologicals—various growth and differentiation factors, antiseptics, and other drugs/biomolecular agonists are either added to the cell culture media or released from the substrate over time; the cells' DNA is modified to express or knockout a certain feature of interest; foreign microorganisms are introduced to produce synergic interactions and signaling queues; and (C) physicomechanical—shaking, mechanical loads, etc. are applied to enhance the cultures due to a stimulatory effect that they have on the cells.<sup>45</sup>

However, the overarching limitation of these fabricationbased controls is that they are either static, in the sense that they do not vary over time (e.g., substrate material, shape), or are "blind" (a.k.a., open-loop), as in the case of the timed-drug release from the substrate material. In other words, the stimuli do not adapt in response to the cell behavior. Furthermore, after the cells are either seeded or bioprinted into the culture, they cannot be targeted precisely. Consequently, only bulk level monitoring (e.g., probing the temperature and the pH of the bioreactor effluent) and controls (e.g., adjusting the media contents and the bioreactor environment) are available during the culturing stage of the biomanufacturing. So, the culturebased controls are not only poor in the sense that there is little feedback available, but also they have a negligible spatial resolution as well. Yet, precise closed-loop controls over the localized cell behavior throughout the entire culturing process are necessary for producing viable and consistent biological products. For example, in vivo organogenesis occurs in multiple steps; this is illustrated by how most bones in our bodies start out as cartilage and only subsequently become calcified through a process called endochondral ossification. Thus, to replicate such dynamic biological processes in vitro, both spatial and temporal controls over the culture development are required.

For this reason, several attempts have been made in the past to create the microfluidic culturing devices; <sup>9–17</sup> most notably, Prof. Robert Langer's, <sup>10</sup> who is regarded as one of the founders of bioengineering. However, the past works focused primarily on developing materials for this purpose, <sup>9–17</sup> while the microfluidic plumbing necessary for the targeted minimally disruptive fluid and cell manipulations at different locations within the artificial culture constructs has not been designed. To that end, we hypothesized that an addressable plumbing design, commonly used for high-throughput microfluidic assays, could be modified to enable the minimally disruptive cell and/or chemical delivery and/or removal/sampling, at targeted locations within the living

I

artificial cultures. As a proof-of-concept, we fabricated a prototype, which can perform the said operations within a 2D microfluidic device (though the ultimate goal is to extend this technology to 3D). Furthermore, we automated the platform, to eliminate the reliance on human labor over the long-term culturing periods, which are typically expected in biological experiments. Consequently, we have shown that the device is capable of a localized payload (both fluids and cells) delivery and sampling, directly below any desired address. Furthermore, we have used this technology to demonstrate that it is capable of both additive and subtractive manufacturing, by creating various co-culture seeding patterns and using flow-focused trypsin delivery to detach the cells at the user-selected locations. None of these operations are currently possible in cell cultures fabricated using conventional means (e.g., bioprinting)- because all access to the cells is lost after they have been deposited into the intended positions.

Yet, the resolution with which the cultures could be created and patterned using our technology is already comparable to that of the bioprinters. Moreover, it could be improved even further by scaling down the plumbing features to smaller sizes via advanced fabrication techniques and by introducing machine vision algorithms into the automation software, to increase the cell trapping precision via the O-valve beyond what is currently practical manually. Hence, in principle, single-cell behavior such as migration, differentiation, proliferation, and ECM deposition could all be controlled using this approach, throughout the entire culturing process, which is currently not possible using the existing technologies. Moreover, this complementary "marriage" between microfluidics and cell substrates would blur the line between fabrication and culturing stages of the biomanufacturing process. Instead, it would make the entire process continuous, thereby allowing to retain the precision, and the control over the individual cells in the device, well into the culturing stage.

However, there are still technological difficulties that need to be overcome to advance the 2D prototype to a fully fledged 3D culturing device, namely, (1) the addressable microfluidic plumbing needs to be scaled up to XYZ delivery/sampling (instead of just XY); (2) to facilitate mass production of the addressable microfluidic cell culturing platforms, a manufacturing method that is free of manual layer-by-layer alignment needs to be developed. There are several potential candidate technologies that could be used for this in the near future. For example, digital micromirror device projection printing (DMD-PP) is a stereolithographic method that uses an array of micromirrors to spatially modulate a pulsed UV laser, to achieve additive cross-linking patterns in a photocurable material. 14,46-49 Similarly, it can also be used for subtractive laser ablation within previously cross-linked layers of the material. While an alternative approach is to 3D print a sacrificial mold (a.k.a. "template"), shaped like the inverse of the desired pore network. 13 The template is then submerged into a gel precursor of the substrate material. After the gel has solidified around the template, the latter is dissolved out of the gel, leaving behind the desired porous networks in the device. (3) Finally, the device should be biocompatible and biodegradable when implanted in vivo. As mentioned before, there are a number of candidate materials that have been custom-designed specifically for the purpose of fabricating microfluidic cultures, such as poly(Llactic-co-glycolic) (PLGA), poly(glycerol-co-sebacate) (PGS), silk fibroin, poly(ester amide), poly(1,3-diamino-2-hydroxypropane-co-polyol sebacate) (APS),12 poly(ethylene glycol)diacrylate (PEGDA), <sup>13</sup> poly(octamethylene maleate (anhydride) citrate) (POMaC), <sup>15</sup> and di-acrylated pluronic F127 (F127-DA). <sup>17</sup> However, given that the plumbing in these studies did not utilize the use of microfluidic valves, it is not apparent whether these materials are stiff enough to make them. Only the silk fibroin has been used to create such valves, but it is not a cross-linkable material, <sup>16</sup> so it is currently not compatible with the 3D stereolithographic fabrication methods such as the DMD-PP. Therefore, further work should be done to test the mechanical properties of these candidate materials or develop new cross-linkable, biodegradable/biocompatible materials that are stiff enough to create the microfluidic valves and that would ideally be also optically transparent for microscopy observation.

Overall, the successful development of the microfluidic cultures will help to minimize the crippling product variability plaguing the biomanufacturing industry today. This will generally benefit the studies of biology, tissue engineering, drug testing, and others. Moreover, the minimally disruptive visual and chemical observation of the cell behavior in the artificial cultures will lower experiment costs and provide datagathering continuity superior to the conventional analysis (i.e., destructive assays for each time point). Ultimately, the proposed approach could pave the way toward tracking and controlling every cell in a culture on an individual basis, given that its targeting precision is limited only by the fabrication resolution of the microfluidic plumbing features (to be refined tremendously by the anticipated explosion of the 3D printers<sup>6,7</sup>). It is expected that this will shift the biomanufacturing paradigm from integrating blind (i.e., open-loop) controls into the culture's substrate material (e.g., timed-drug release) to controlling the cells in growing biological constructs interactively instead. Finally, the computer-driven culturing would solve a major logistical hurdle to the adoption of such technologies by allowing companies to provide digital codes to hospital staff, instead of having to teach them a different custom culturing protocol for each new product (which is impractical). Therefore, this technology would both simplify the process for the end user and ensure specification compliance on site.

# **V. CONCLUSIONS**

We have presented a microfluidic platform capable of performing spatiotemporal manipulations of fluids and cells within living cultures. Specifically, we have interlaced a PDMS prototype with addressable microfluidic ports and demonstrated that it is capable of delivering/sampling fluids in the culture chamber situated at the bottom of the chip. Furthermore, we have shown its ability to perform additive manufacturing by creating spatial cell seeding patterns by flowing fluorescent MSCs and NIH/ 3T3s into different locations within the device. Moreover, we also demonstrated subtractive manufacturing by detaching selected cells via localized trypsin delivery and flushing them from the culture chamber. Finally, we showed that the detached cells can also be captured and sent off for ex situ assaying, thereby overcoming the need for destructive analysis that is common in biological studies. Although the proof-of-concept device demonstrated in this manuscript was only 2D, in the future we plan to extend this concept to XYZ manipulations within transparent, biocompatible, and biodegradable 3D cultures. It is our hope that the design will ultimately resolve the bottlenecks plaguing the conventional biomanufacturing technologies today and ultimately enable computer-driven cell culturing through coupling with automation electronics.

Specifically, the proposed technology would enable: (1) improved nutrient delivery and metabolic waste removal within thick cultures; (2) viable and consistent products via orchestration of cell action during culturing; (3) improved drug screening via nondestructive sampling of cell responses throughout the entire time course of administration; (4) biomanufacturing automation for achieving desired specifications on site, without the need to train hospital staff custom culturing protocols for every different cell culture product and experiment.

#### ASSOCIATED CONTENT

# Supporting Information

The Supporting Information is available free of charge at https://pubs.acs.org/doi/10.1021/acsbiomaterials.9b01969.

Demonstration of ex situ sacrificial phenotypic assaying of MSC-differentiated osteoblasts biopsied from the microfluidic device via its addressable ports (Figure S1) (PDF) Proof-of-concept demonstration of the device's ability to manipulate fluids at different XY locations within the culture chamber (Video S1) (MP4)

Proof-of-concept demonstration of the device's ability to seed cells at user-specified locations within the culture chamber (Video S2) (MP4)

Proof-of-concept demonstration of the device's cell manipulation precision (Video S3) (MP4)

Proof-of-concept demonstration of the device's ability to perform minimally disruptive cell subtractions within the culture chamber (Video S4) (MP4)

Proof-of-concept demonstration of the device's ability to collect minimally disruptive cell biopsies from the culture chamber (Video S5) (MP4)

# AUTHOR INFORMATION

# **Corresponding Author**

Roman Voronov — Otto H. York Department of Chemical and Materials Engineering and Department of Biomedical Engineering, New Jersey Institute of Technology, Newark College of Engineering, Newark, New Jersey 07102, United States; orcid.org/0000-0001-6685-949X; Phone: +1 973 642 4762; Email: rvoronov@njit.edu; Fax: +1 973 596 8436

#### **Authors**

**Anh Tong** — Otto H. York Department of Chemical and Materials Engineering, New Jersey Institute of Technology, Newark College of Engineering, Newark, New Jersey 07102, United States;

orcid.org/0000-0001-9475-5137

Quang Long Pham — Otto H. York Department of Chemical and Materials Engineering, New Jersey Institute of Technology, Newark College of Engineering, Newark, New Jersey 07102, United States; Department of Biomedical Engineering, Tufts University, Medford, Massachusetts 02155, United States; orcid.org/0000-0003-4010-5408

Vatsal Shah — Department of Computer Science, Ying Wu College of Computing Sciences and Federated Department of Mechanical and Industrial Engineering, New Jersey Institute of Technology, Newark College of Engineering, Newark, New Jersey 07102, United States; ○ orcid.org/0000-0002-9638-4701

Akshay Naik — Helen and John C. Hartmann Department of Electrical and Computer Engineering, New Jersey Institute of Technology, Newark College of Engineering, Newark, New Jersey 07102, United States; orcid.org/0000-0002-6155-2218

Paul Abatemarco — Otto H. York Department of Chemical and Materials Engineering, New Jersey Institute of Technology, Newark College of Engineering, Newark, New Jersey 07102, United States; ⊚ orcid.org/0000-0002-8126-6921

Complete contact information is available at: https://pubs.acs.org/10.1021/acsbiomaterials.9b01969

#### Notes

The authors declare no competing financial interest. This article does not contain any studies with human participants or animals performed by any of the authors.

#### ACKNOWLEDGMENTS

The authors would like to thank Gustavus and Louise Pfeiffer Research Foundation Major Investment Grant, New Jersey Health Foundation Research Award—Grant #PC 22-19, NJIT Faculty Seed Grant, NSF I-Corps Site—Grant #1450182 for their gracious funding of their work. Additionally, the authors would like to thank NSF XSEDE EMPOWER, and New Jersey Institute of Technology (NJIT)'s McNair Achievement and Provost Summer Research Programs for funding student labor for this project. Futhermore, the authorswould like to thank Dr. Rafael Gómez-Sjöberg for providing software and blueprints for the automated pneumatic pumping technology. Moreover, the authors would like to thank Ph.D. candidate Thanh Danh Nguyen for contributing to Figure 1. Also, the authors would also like to thank NJIT's Profs. Edward Dreyzin, Treena Arinzeh, and Gal Haspel for the invaluable discussions. Finally, the authors acknowledge that the computational resources used in this study were provided by the New Jersey Institute of Technology's Academic and Research Computing Systems (ARCS) and by the Texas Advanced Computing Center (TACC) at the University of Texas at Austin through the Campus Champions program within the Extreme Science and Engineering Discovery Environment (XSEDE).<sup>50</sup> The latter is supported by the National Science Foundation's grant number ACI-1548562.

# ABBREVIATIONS

HMDS, hexamethyldisilazane; PDMS, poly(dimethylsiloxane) Sylgard 184; ECM, Extracellular Matrix; BSA, bovine serum albumin; MEM, minimum essential medium; FBS, fetal bovine serum; MSCs, mesenchymal stem cells; NIH/3T3s, mouse embryo fibroblasts; EDTA, ethylenediaminetetraacetic acid; PBS, phosphate-buffered saline

# REFERENCES

- (1) Hunter, R. 3D Cell Culture: Technologies and Global Markets, 2017.
- (2) Breslin, S.; O'Driscoll, L. Three-dimensional cell culture: the missing link in drug discovery. *Drug Discovery Today* **2013**, *18*, 240–249.
- (3) Ye, K.; Kaplan, D. L.; Bao, G.; Bettinger, C.; Forgacs, G.; Dong, C.; Khademhosseini, A.; Ke, Y.; Leong, K.; Sambanis, A.; Sun, W.; Yin, P. Advanced Cell and Tissue Biomanufacturing. *ACS Biomater. Sci. Eng.* **2018**, *4*, 2292–2307.
- (4) Wu, P. H.; Giri, A.; Sun, S. X.; Wirtz, D. Three-dimensional cell migration does not follow a random walk. *Proc. Natl. Acad. Sci. U.S.A.* **2014**, *111*, 3949–3954.
- (5) Dlouhy, B. J.; Awe, O.; Rao, R. C.; Kirby, P. A.; Hitchon, P. W. Autograft-derived spinal cord mass following olfactory mucosal cell transplantation in a spinal cord injury patient: Case report. *J. Neurosurg. Spine* **2014**, *21*, 618–622.

- (6) Hunsberger, J.; Harrysson, O.; Shirwaiker, R.; Starly, B.; Wysk, R.; Cohen, P.; Allickson, J.; Yoo, J.; Atala, A. Manufacturing road map for tissue engineering and regenerative medicine technologies. *Stem Cells Transl. Med.* **2015**, *4*, 130–135.
- (7) Naderi, A.; Bhattacharjee, N.; Folch, A. Digital Manufacturing for Microfluidics. *Annu. Rev. Biomed. Eng.* **2019**, *21*, 325–364.
- (8) Bhattacharjee, N.; Urrios, A.; Kang, S.; Folch, A. The upcoming 3D-printing revolution in microfluidics. *Lab Chip* **2016**, *16*, 1720–1742.
- (9) King, K. R.; Wang, C. C. J.; Kaazempur-Mofrad, M. R.; Vacanti, J. P.; Borenstein, J. T. Biodegradable microfluidics. *Adv. Mater.* **2004**, *16*, 2007–2012.
- (10) Bettinger, C. J.; Weinberg, E. J.; Kulig, K. M.; Vacanti, J. P.; Wang, Y.; Borenstein, J. T.; Langer, R. Three-dimensional microfluidic tissuengineering scaffolds using a flexible biodegradable polymer. *Adv. Mater.* **2006**, *18*, 165–169.
- (11) Bettinger, C. J.; Cyr, K. M.; Matsumoto, A.; Langer, R.; Borenstein, J. T.; Kaplan, D. L. Silk Fibroin Microfluidic Devices. *Adv. Mater.* **2007**, *19*, 2847–2850.
- (12) Wang, J.; Bettinger, C. J.; Langer, R. S.; Borenstein, J. T. Biodegradable microfluidic scaffolds for tissue engineering from amino alcohol-based poly (ester amide) elastomers. *Organogenesis* **2010**, *6*, 212–216.
- (13) Miller, J. S.; Stevens, K. R.; Yang, M. T.; Baker, B. M.; Nguyen, D.-H. T.; Cohen, D. M.; Toro, E.; Chen, A. A.; Galie, P. A.; Yu, X. Rapid casting of patterned vascular networks for perfusable engineered 3D tissues. *Nat. Mater.* **2012**, *11*, 768.
- (14) Cha, C.; Soman, P.; Zhu, W.; Nikkhah, M.; Camci-Unal, G.; Chen, S.; Khademhosseini, A. Structural Reinforcement of Cell-Laden Hydrogels with Microfabricated Three Dimensional Scaffolds. *Biomater. Sci.* **2014**, *2*, 703–709.
- (15) Zhang, B.; Montgomery, M.; Pahnke, A.; Reis, L.; Nunes, S. S.; Radisic, M. In *Microfluidic Tissue: A Biodegradable Scaffold with Built-in Vasculature for Cardiac Tissue Vascularization and Surgical Vascular Anastomosis*, Proceedings of the Seventeenth International Conference on Miniaturized Systems for Chemistry and Life Sciences, 2013; pp 2019–2021.
- (16) Zhao, S.; Chen, Y.; Partlow, B. P.; Golding, A. S.; Tseng, P.; Coburn, J.; Applegate, M. B.; Moreau, J. E.; Omenetto, F. G.; Kaplan, D. L. Bio-functionalized silk hydrogel microfluidic systems. *Biomaterials* **2016**, *93*, 60–70.
- (17) Shen, C.; Li, Y.; Wang, Y.; Meng, Q. Non-swelling hydrogel-based microfluidic chips. *Lab Chip* **2019**, *19*, 3962–3973.
- (18) Wang, H. Y.; Bao, N.; Lu, C. A microfluidic cell array with individually addressable culture chambers. *Biosens. Bioelectron.* **2008**, 24, 613–617.
- (19) Leung, K.; Zahn, H.; Leaver, T.; Konwar, K. M.; Hanson, N. W.; Page, A. P.; Lo, C. C.; Chain, P. S.; Hallam, S. J.; Hansen, C. L. A programmable droplet-based microfluidic device applied to multiparameter analysis of single microbes and microbial communities. *Proc. Natl. Acad. Sci. U.S.A.* **2012**, *109*, 7665–7670.
- (20) Gao, Y.; Tian, J.; Wu, J.; Cao, W.; Zhou, B.; Shen, R.; Wen, W. Digital microfluidic programmable stencil (DMPS) for protein and cell patterning. *RSC Adv.* **2016**, *6*, No. 101760.
- (21) Thorsen, T.; Maerkl, S. J.; Quake, S. R. Microfluidic large-scale integration. *Science* **2002**, *298*, 580–584.
- (22) Melin, J.; Quake, S. R. Microfluidic large-scale integration: the evolution of design rules for biological automation. *Annu. Rev. Biophys. Biomol. Struct.* **2007**, *36*, 213–231.
- (23) Mark, D.; Haeberle, S.; Roth, G.; von Stetten, F.; Zengerle, R. Microfluidic lab-on-a-chip platforms: requirements, characteristics and applications. *Chem. Soc. Rev.* **2010**, *39*, 1153–1182.
- (24) Araci, I. E.; Brisk, P. Recent developments in microfluidic large scale integration. *Curr. Opin. Biotechnol.* **2014**, *25*, 60–68.
- (25) Unger, M. A.; Chou, H. P.; Thorsen, T.; Scherer, A.; Quake, S. R. Monolithic microfabricated valves and pumps by multilayer soft lithography. *Science* **2000**, *288*, 113–116.
- (26) Pham, Q. L.; Tong, N. A. N.; Mathew, A.; Basuray, S.; Voronov, R. S. A compact low-cost low-maintenance open architecture mask

- aligner for fabrication of multilayer microfluidics devices. *Biomicrofluidics* **2018**, 12, No. 044119.
- (27) Li, X.; Yu, Z. T.; Geraldo, D.; Weng, S.; Alve, N.; Dun, W.; Kini, A.; Patel, K.; Shu, R.; Zhang, F.; Li, G.; Jin, Q.; Fu, J. Desktop aligner for fabrication of multilayer microfluidic devices. *Rev. Sci. Instrum.* **2015**, 86, No. 075008.
- (28) Gómez-Sjöberg, R.; Leyrat, A. A.; Pirone, D. M.; Chen, C. S.; Quake, S. R. Versatile, fully automated, microfluidic cell culture system. *Anal. Chem.* **2007**, *79*, 8557–8563.
- (29) Brower, K.; Puccinelli, R.; Markin, C. J.; Shimko, T. C.; Longwell, S. A.; Cruz, B.; Gomez-Sjoberg, R.; Fordyce, P. M. An Open-Source, Programmable Pneumatic Setup for Operation and Automated Control of Single- and Multi-Layer Microfluidic Devices. *HardwareX* **2018**, 3, 117–134.
- (30) Gómez-Sjöberg, R. Rafael's Microfluidics Page. https://sites.google.com/site/rafaelsmicrofluidicspage/home.
- (31) Pham, Q. L.; Chege, D.; Dijamco, T.; Surblyte, M.; Naik, A.; Campbell, K.; Tong, N.-A.-N.; Voronov, R. Open-Source Matlab-Based Graphical User Interface (GUI) For Computer Control of Microscopes Using Micro-Manager, 2019. arXiv:1904.13231. arXiv.org e-Print archive. https://arxiv.org/abs/1904.13231.
- (32) Giang, U.-B. T.; King, M. R.; DeLouise, L. A. Microfabrication of bubbular cavities in PDMS for cell sorting and microcell culture applications. *J. Bionic Eng.* **2008**, *5*, 308–316.
- (33) Shrirao, A. B.; Kung, F. H.; Yip, D.; Firestein, B. L.; Cho, C. H.; Townes-Anderson, E. A Versatile Method of Patterning Proteins and Cells. *J. Visualized Exp.* **2017**, *120*, No. e55513.
- (34) Schneider, C. A.; Rasband, W. S.; Eliceiri, K. W. NIH Image to Image]: 25 years of image analysis. *Nat. Methods* **2012**, *9*, 671–675.
- (35) Park, J. A.; Yoon, S.; Kwon, J.; Now, H.; Kim, Y. K.; Kim, W.-J.; Yoo, J.-Y.; Jung, S. Freeform micropatterning of living cells into cell culture medium using direct inkjet printing. *Sci. Rep.* **2017**, 7, No. 14610.
- (36) Stamm, A.; Reimers, K.; Strauß, S.; Vogt, P.; Scheper, T.; Pepelanova, I. In vitro wound healing assays—state of the art. *BioNanoMaterials* **2016**, *17*, 79—87.
- (37) Felder, M.; Sallin, P.; Barbe, L.; Haenni, B.; Gazdhar, A.; Geiser, T.; Guenat, O. Microfluidic wound-healing assay to assess the regenerative effect of HGF on wounded alveolar epithelium. *Lab Chip* **2012**, *12*, 640–646.
- (38) Wei, Y.; Chen, F.; Zhang, T.; Chen, D.; Jia, X.; Wang, J.; Guo, W.; Chen, J. A Tubing-Free Microfluidic Wound Healing Assay Enabling the Quantification of Vascular Smooth Muscle Cell Migration. *Sci. Rep.* **2015**, *5*, No. 14049.
- (39) Nie, F.-Q.; Yamada, M.; Kobayashi, J.; Yamato, M.; Kikuchi, A.; Okano, T. On-chip cell migration assay using microfluidic channels. *Biomaterials* **2007**, 28, 4017–4022.
- (40) van der Meer, A. D.; Vermeul, K.; Poot, A. A.; Feijen, J.; Vermes, I. A microfluidic wound-healing assay for quantifying endothelial cell migration. *Am. J. Physiol.: Heart Circ. Physiol.* **2010**, 298, H719–H725.
- (41) Huang, X.; Li, L.; Tu, Q.; Wang, J.; Liu, W.; Wang, X.; Ren, L.; Wang, J. On-chip cell migration assay for quantifying the effect of ethanol on MCF-7 human breast cancer cells. *Microfluid. Nanofluid.* **2011**, *10*, 1333–1341.
- (42) Conant, C. G.; Nevill, J. T.; Schwartz, M.; Ionescu-Zanetti, C. Wound Healing Assays in Well Plate—Coupled Microfluidic Devices with Controlled Parallel Flow. *JALA* **2010**, *15*, 52–57.
- (43) Murrell, M.; Kamm, R.; Matsudaira, P. Tension, free space, and cell damage in a microfluidic wound healing assay. *PLoS One* **2011**, *6*, No. e24283.
- (44) Zeng, J.; Mohammadreza, A.; Gao, W.; Merza, S.; Smith, D.; Kelbauskas, L.; Meldrum, D. R. A minimally invasive method for retrieving single adherent cells of different types from cultures. *Sci. Rep.* **2014**, *4*, No. 5424.
- (45) Fernandez-Yague, M. A.; Abbah, S. A.; McNamara, L.; Zeugolis, D. I.; Pandit, A.; Biggs, M. J. Biomimetic approaches in bone tissue engineering: Integrating biological and physicomechanical strategies. *Adv. Drug Delivery Rev.* **2015**, *84*, 1–29.

- (46) Warner, J.; Soman, P.; Zhu, W.; Tom, M.; Chen, S. Design and 3D Printing of Hydrogel Scaffolds with Fractal Geometries. *ACS Biomater. Sci. Eng.* **2016**, *2*, 1763–1770.
- (47) Zhang, A. P.; Qu, X.; Soman, P.; Hribar, K. C.; Lee, J. W.; Chen, S.; He, S. Rapid fabrication of complex 3D extracellular microenvironments by dynamic optical projection stereolithography. *Adv. Mater.* **2012**, 24, 4266–4270.
- (48) Hribar, K. C.; Soman, P.; Warner, J.; Chung, P.; Chen, S. Light-assisted direct-write of 3D functional biomaterials. *Lab Chip* **2014**, *14*, 268–275
- (49) Yang, W.; Yu, H.; Liang, W.; Wang, Y.; Liu, L. Rapid fabrication of hydrogel microstructures using UV-induced projection printing. *Micromachines* **2015**, *6*, 1903–1913.
- (50) Towns, J.; Cockerill, T.; Dahan, M.; Foster, I.; Gaither, K.; Grimshaw, A.; Hazlewood, V.; Lathrop, S.; Lifka, D.; Peterson, G. D. XSEDE: accelerating scientific discovery. *Comput. Sci. Eng.* **2014**, *16*, 62–74.